Igor Esau[1*], Victoria Miles[1]
[1] Nansen Environmental and Remote Sensing Centre/Bjerknes Centre for Climate Research, Bergen, Norway
*** Corresponding author:** igore@nersc.no

EXOGENOUS DRIVERS OF SURFACE URBAN HEAT ISLANDS IN NORTHERN WEST SIBERIA

ABSTRACT. Urban temperature anomalies, frequently referred to as the urban heat islands (UHIs), are of the most distinct and influential climatic factors with significant impact on urban life and environment. However, UHIs in high latitudes are still studied only fragmentary. There is a knowledge gap related to the urban temperature distinction with respect to local temperature anomalies of natural surface types. This study extends upon our recent high latitude regional-scale climatic survey in 28 cities in the Northern West Siberia (NWS) region. Based on MODIS land surface temperature (LST) products covering 15 years between 2001 and 2015, it was revealed that all 28 cities have significant surface urban heat islands (SUHIs). The strong statistical dependence (r = 0.73) on endogenous factors such as city size and the population was found. It was suggested that exogenous factors such as the background LC types could be significant as well. This study presents the analysis of the exogenous factors shaping the apparent SUHI intensities. The major contribution to the SUHI was revealed for water, sparse vegetation, grassland, and shrubland. There are no clear dependence between the partial SUHI intensity and the area fraction occupied by the given LC type. The mechanisms and pathways of the SUHI maintenance cannot be inferred solely from the remote sensing data. Further understanding requires numerical experiments with turbulence-resolving models.

KEY WORDS: Surface Urban Heat Island, Remote sensing, MODIS, Siberia, Exogenous factors of urban climate, Sustainable urban development

CITATION: Igor Esau, Victoria Miles (2018) Exogenous Drivers Of Surface Urban Heat Islands In Northern West Siberia. Geography, Environment, Sustainability, Vol.11, No 3, p. 83-99
DOI-10.24057/2071-9388-2018-11-3-83-99

INTRODUCTION

Microclimates of anthropogenic and natural landscapes can significantly deviate from the regional climate. Anthropogenic landscapes dominate urban and industrial areas where the economic and cultural values of our societies are concentrated. These values induce the need to characterize urban microclimates and to distinguishes them from microclimates of the surrounding natural landscapes. An urban microclimate is typically warmer than that outside of the city margins. This phenomenon is widely referred to as an urban heat island (UHI), or, more specifically, as a surface urban heat island (SUHI) when the land surface temperature (LST) is considered (Voogt and Oke 2003). It should be noted that even the most rigorous studies are somewhat vague

on definition of urban and rural temperature observations (Lowry 1977); as they might be affected by the urban boundary layer footprint (Tomlinson et al. 2012).

Following urban climate literature, the UHI intensity could be defined as a temperature difference

$$\Delta T = T_u - T_r \quad (1)$$

between the urban and rural sites. The choice of proper sites is however never trivial. Both urban and natural microclimates are geographically fragmented. Both T_u and T_r vary strongly from site to site. Stewart (2011) proposed a set of reasonable criteria to organize inter-comparable surface air temperature (SAT) measurements in the UHI studies. Those criteria are however not universal and would probably not meet the needs of many practical tasks.

Satellite observations and remote-sensing data sets open an opportunity to study urban microclimate with spatially dense and regular meteorological data. In this case, T_u , T_r and ΔT could be understood correspondingly as the urban and rural LST and the SUHI intensity. Schwartz et al. (2011) compared 11 approaches for quantifying SUHI with the Moderate Resolution Imaging Spectroradiometer (MODIS) LST data for European cities. The study showed that the resulting SUHI intensity is strongly sensitive to the choice of both urban and rural pixels as well as the calculation methods.

Effective utilization of the urban microclimate information in decision-making processes is impossible without understanding of the UHI driving factors, mechanisms and variability. Such studies require internally homogeneous, intercomparable ΔT data sets to retrieve the effects of different endogenous factors, i.e. those induced by the urban characteristics itself, and *exogenous* factors, i.e. those induced by the characteristics of the surrounding natural background. The endogenous factors change T_u. Among the most common endogenous factors, one may find dependences on the percent of impervious surface area (ISA) (e.g. Li et al. 2018), the city area and population (e.g. Oke 1973; Sun and Lin 2005; Mokhov 2009; Shastri et al. 2017). For example, a high correlation between T_u from the MODIS LST and ISA was shown in Minneapolis (USA) (Yuan and Marvin 2007). Smoliak et al. (2015) took this correlation into account redefining the UHI as the urban-airport temperature difference. Their approach separates the anthropogenic flux contribution but is inconsistent with observations requirements for the natural background temperatures. A wider study by Imhoff et al. (2010) concluded that the ISA alone could explain up to 70% of the total LST variance in 38 the most populous US cities. Zhang et al. (2010) found that 60% of the total LST variance could be explained by the ISA for the cities within a high-latitude forest zone.

The exogenous factors induce changes in T_r. In many cases, the endogenous factors alone cannot characterize the urban microclimate and the anthropogenic contribution in its formation. Hu and Jia (2010) found expansion of the positive temperature anomalies with land use – land cover changes in China. They noted that the temperature observations are very sensitive to the placement of a meteorological station. Zhao et al. (2014) studied major North American cities and concluded that the exogenous factors, such as the local background climate, strongly influence the UHI intensity. The urban temperature anomalies, ΔT, were-largely explained by variations in the air-land heat exchange within the atmospheric boundary layer – canopy – upper soil system. This efficiency is largely controlled by the physical climatic factors of the surrounding natural background, which include aerodynamic surface roughness, soil heat capacity, surface albedo and evapotranspiration properties. As the physical factors are difficult and expensive to measure and quantify, geographical climatic factors, e.g. land cover (LC) types, are more widely applied (e.g. He et al. 2010). Yang et al. (2017) reviewed the influence of background landscape on the SUHI intensity in 332 Chinese cities across several climate zones. In the study, LC types were retrieved from satellite observations and used to identify the profound effects of the natural microclimatic factors on the LST. The most significant impact was attributed

to vegetation classes such as forest, grassland and cultivated land. The overall effect was that the UHI in humid forested landscapes is less intensive than in open dry ones.

There are good reasons to expect that the exogenous factors are similarly or even more effective in scaling the SUHI intensity in high latitudes. There are often more contrasting landscapes of dark coniferous forest and open grassland. The natural local temperature differences could be large and persistent (Li et al. 2015), while snow cover may exacerbate differences in the surface radiative balance (Lemonsu et al. 2008; Dudorova and Belan 2015; Mori and Sato 2015). There is strong competition between sensible and latent fluxes for additional heating, whereas the balance could be skewed by small changes in soil moisture (Brunsell et al. 2011; Barichivich et al. 2014). Moreover, the additional heat is usually trapped near the surface in the stably stratified atmosphere, raising the temperature more than it would be observed at lower latitudes (Davy and Esau 2016; Davy et al. 2017).

The SUHI in the boreal regions have received some attention only in recent years. Before the Miles and Esau (2017) study, hereafter referred to as ME17, the published remote sensing studies had not extended north of 60°N (Zhang et al. 2010; Peng et al. 2012; Clinton and Gong 2013). There were however a few available in situ studies addressing the UHI in the high-latitude cities (Magee 1999; Hinkel and Nelson 2007; Varentsov et al. 2014; Konstantinov et al. 2015). The most recent in situ study by Konstantinov et al. (2018) have addressed the UHI in 3 cities in Northern Western Siberia (NWS). Both the ME17 and Konstantinov et al. (2018) studies revealed rather large intensity of the urban LST and air temperature anomalies with peak values exceeding 10K. The seasonally averaged SUHI intensities are however less extreme. They vary between 0.5K to 2.5K in most cases in both seasons. Moreover, the SUHI in NWS demonstrates a rather unusual behaviour, with larger wintertime and nocturnal intensities.

In this study, we investigate the *exogenous* factors affecting, and therefore, contributing to the large scatter and unusual behaviour of the SUHI intensities found in the 28 NWS cities. Although such exogenous factors of the SUHI received little attention in literature, there is a growing demand to assess them and determine their role in shaping urban microclimates. This demand is driven by the observed and suggested SUHI impact on related physical, ecological and socio-economic processes (Makhrovskaya et al. 1977; Lapenis et al. 2005; Khrustalyov and Davidova 2007; Heleniak 2009; Grebenets et al. 2012; Streletskiy et al. 2012; Shiklomanov et al. 2016; Esau and Miles 2016). There are strong physical reasons to expect that the cold continental climate in NWS exacerbates the microclimatic distinction, trapping heat in a shallow urban boundary layer of the stably stratified lower atmosphere (Davy and Esau 2016; Davy et al. 2017). This study is based on the same data sets as ME17, but its focus shifts to the spatial composition with respect to selected land cover types. The data represent the period between 2001 and 2015.

MATERIALS AND METHODS

The study area

The NWS region has the largest concentration of small and medium cities in severe continental climate across several bioclimatic zones of high latitudes. This region includes the territory of two administrative districts (okrugs): Yamalo-Nenets Autonomous Okrug and Khanty–Mansi Autonomous Okrug. The NWS landscape is flat and homogeneous. However, at the city scales, the land cover could be rather heterogeneous and fragmented. The surface elevations are typically less than 100 meters above the sea level. The low, flat surface and large surface humidity result in widespread paludification of the region; in some parts, swamps cover up to 80%. Forest covers only 36% of the area.

Climate of the region is of the Dfc type (cold, fully humid climate with snow) according to the Koeppen-Geiger classification (Kottek et al. 2006). The mean winter surface temperature and amount of snow decrease in the northeastern direction, according to

the Russian National Atlas (http://национальныйатлас.рф). Winters are cold with the stable snow cover from October through April (200 to 230 days per annum). The mean January temperatures vary between –22°C and –29°C. The mean July temperatures are distributed more uniformly with a south-north temperature decrease from +17°C (in the cities along the middle Ob river) to +14°C (in the northernmost cities). The mean annual surface air temperatures are between –2°C to –9°C. At the same time, permafrost remains isolated, sporadic and discontinuous due to significant snow depth (about 150 cm by the end of the season), according to the International Permafrost Association (https://ipa.arcticportal.org/). The cloud cover in the region is moderate (60%) with a large number of the clear-sky days (1600 hours of the annual sunshine), particularly in the winter season. Thus, the regional climate is beneficial to the application of remotely sensed data sets.

The MODIS LST data products

This study utilizes the LST data from the Moderate Resolution Imaging Spectroradiometer (MODIS), which provides an opportunity for the region-scale analysis of the SUHI. The MODIS data has high calibration accuracy in multiple thermal infrared bands designed for retrievals of the LST and atmospheric properties (Wang 2008). The LST products from the MODIS sensors aboard the Terra (EOS AM) and Aqua (EOS PM) satellites have been already widely used for the urban climate studies (e.g., Imhoff et al. 2010; Clinton and Gong 2012; Peng 2012). It has been shown that the MODIS LST have high correlations with the in situ measured soil temperature for different northern land cover types (Muster et al. 2015) and with the surface air temperature measured at the height of 2 m above the ground (Comiso 2003; Jin and Dickinson 2010; Hachem et al. 2012). Although the MODIS LST is observed only under the clear-sky weather conditions, it is generally representative for climatic LST studies (Chen et al. 2017), especially when the gap filling in larger areas is applied (Yang et al. 2017; Metz et al. 2017). We continue the discussion of the LST – SAT differences in the high latitudes in the next section.

This study considers the thermal anomaly associated with urban areas using the Terra/MODIS LST product MOD11A2. MOD11A2 is an 8-day LST product by averaging from two to eight days of the clear sky MOD11A1 daily product and has 12 Science Data Sets (SDS) layers (Li 2013). A split-window algorithm is used for calculating the LST. The day/night LST method retrieves land-surface temperature and band emissivity simultaneously from pairs of daytime and night-time MODIS data scenes in seven TIR bands. The LST composites were downloaded from http://reverb.echo.nasa.gov/. The data were re-projected from the Sinusoidal projection to the UTM Zone 42N projection system with the WGS84 datum. The data were also reformatted from HDF-EOS to GeoTIFF and converted from °K to °C. According to the product quality control flag, the utilized data have an average LST error ≤ 2°C.

This study considers data collected between 2001 and 2015. The analysis has been carried out for winter (December, January and February, DJF) and summer (June, July and August, JJA) seasons. We processed day and night LST data for the Terra/MODIS overpass times at approximately 10:30 and 22:30 local time.

The SUHI definition

The SUHI intensity, ΔT , is defined by Eq. 1 in this study. The ME17 study defined the urban temperature, T_u , as the maximal temperature of the urban pixels. The urban pixels were associated with the city area (polygon) given by the administrative city boundaries. The city edge polygons were downloaded from the Russian Demographic Database (http://www.grid.unep.ch/russia/). Because administrative city boundaries differed from the true extents, each polygon was manually corrected using ArcGIS base maps.

The rural temperature, T_r , was defined as the average temperature of the surrounding, non-urban pixels in a 2 km buffer around the city area. Rural pixels were classified as natural surfaces of different LC types. Averaging did not account for the LC types of the rural pixels. But we excluded all pixels related to the urban or artificial surfaces and

water pixels, because these surfaces have significant impact on the mean rural LST. The approach was partially adopted from that by Zhou et al. (2013). Thus, the resulting represented the difference between the maximum temperature of the city and the mean temperature of minimally developed land outside the city. Daytime and nighttime SUHI were calculated separately for winter and summer seasons. They were further averaged to obtain the seasonal mean values. Such SUHI are methodologically similar to the SUHI in the earlier studies by e.g. Peng et al. (2012) and Zhou et al. (2015).

Investigation of the exogenous factors requires a redefinition of the type-specific SUHI intensity as the temperature difference between the maximal urban temperature, T_u, and the temperature average over all pixels of a given LC type, l. Thus, Eq. 1 will be interpreted as

$$\Delta T_l = T_u - T_l \qquad (2)$$

If the fraction of the buffer, which is covered by the LC type l, is f_l where

$$\sum_l f_l = 1 \quad ,$$

then one may recover

$$\Delta T = \sum_l f_l \Delta T_l = T_u - \sum_l f_l T_l = T_u - T_r \qquad (3)$$

where $f_l \Delta T_l$ is the partial contribution of the l-th LC type to the total SUHI intensity. The type-specific SUHI intensity does not necessarily need to be positive. According to the conclusion of Li et al. (2015), the SUHI might be negative relative to the boreal forest LC types.

The land cover data set

This study is based on the LC types from the Climate Change Initiative (CCI) data provided by the European Space Agency (ESA). The data are publicly available. The CCI LC data have the spatial resolution of 300 m. The LC types were obtained from the annual global time series from 1992 to 2015. In this study, we use the data for 2015. The land cover was extracted from CCI LC raster and converted to polygons. The original CCI LC types were aggregated into new 9 more general LC types. Table 1 provides an overview of the CCI LC types that were found around the NWS cities, and aggregated types used in this study. All GIS and remote-sensing data were processed using ArcGIS 10.3 software.

The 28 NWS cities

The study considers 28 NWS cities. The list of cities is given in Table 1. Fig. 1 shows the NWS region with the cities, SUHI intensity and background mean seasonal LST. The majority of the considered settlements exhibit SUHI intensities in the range from 1.5 K to 3.0 K with the extreme wintertime SUHI anomaly in Surgut exceeding 5 K. The seasonally averaged summer SUHI intensities in these cities have small and even negative values in the most northern cities.

The impact of exogenic factors on the SUHI was quantified through calculation of the LST differences between the urban LC type and the specific LC types found in the 2 km buffer around administrative boundaries of each city. This method is given by Eq. 2 and Eq. 3. Fig. 2 gives a visual example of the method applied to the small-size city of Pokachy. It shows the city polygon and the surrounding 2 km buffer covered by different aggregated LC types in 300 x 300 m^2 squares. The numbers show the mean summer (positive) and winter (negative) LST for different LC types. This figure reveals that all LC types have lower LST than the urban area. However, there are significant differences between the LC types. The area is largely covered with sparse vegetation and wetlands. Wetlands are considerably warmer than the other LC types, reducing the specific SUHI by almost 1 K.

Composition of the LC types surrounding the cities

The natural background of the NWS cities is dominated by three LC types: wetland; grassland; and sparse vegetation. Only a few cities are in the background with a large fraction of woodland (Beloyarsky, Purpe, Nyagan and Sovetskiy) and shrubland (Nefteyugansk, Nadym, Labytnangi). Fig. 3 presents the fractions of the LC types for each city. The natural background of many cities

Table 1. The CCI LC types

ID	Aggregated LC types	Original CCI LC type description
10	Cropland	Cropland, rainfed
11	Grassland	Herbaceous cover
30	Cropland	Mosaic cropland (>50%) / natural vegetation (tree, shrub, herbaceous cover) (<50%)
40	Woodland	Mosaic natural vegetation (tree, shrub, herbaceous cover) (>50%) / cropland (<50%)
60	Spare vegetation	Tree cover, broadleaved, deciduous, closed to open (>15%)
70	Spare vegetation	Tree cover, needleleaved, evergreen, closed to open (>15%)
80	Spare vegetation	Tree cover, needleleaved, deciduous, closed to open (>15%)
90	Woodland	Tree cover, mixed leaf type (broadleaved and needleleaved)
100	Shrubland	Mosaic tree and shrub (>50%) / herbaceous cover (<50%)
110	Grassland	Mosaic herbaceous cover (>50%) / tree and shrub (<50%)
120	Shrubland	Shrubland
122	Shrubland	Shrubland deciduous
130	Sparse vegetation	Grassland
140	Spare vegetation	Lichens and mosses
150	Spare vegetation	Sparse vegetation (tree, shrub, herbaceous cover) (<15%)
152	Spare vegetation	Sparse shrub (<15%)
160	Wetland	Tree cover, flooded, fresh or brakish water
180	Wetland	Shrub or herbaceous cover, flooded, fresh/saline/brakish water
190	Artificial land	Urban areas
200	Bare areas	Bare areas
201	Bare areas	Consolidated bare areas
210	Water bodies	Water bodies

is largely covered by one or two LC types. It makes the corresponding SUHI dependent on the local climate of that specific LC type, and therefore, intercomparison becomes sensitive to selection of the cities with similar LC types. A few cities found on a more diverse background. This applies mostly to the older cities (Salekhard/Labytnangi, Khanty-Mansiysk).

Exogenic contribution to the SUHI intensity

We calculated the partial contribution of each aggregated LC type to the total SUHI intensity for the considered 28 cities in the NWS region. The LC type data (Fig. 3) were used to obtain the fractional area, f_I, and the LST data (e.g. as in Fig. 2) – to obtain the LST anomaly, ΔT_I, specific for the given LC type. The method is given in Eq. 3. Fig. 4 shows that some LC types can locally have nearly the same or even higher LST as the urban proper itself.

The apparent SUHI is the most pronounced on the background of spare vegetation and grassland. In some cities, shrubland has also contributed in the SUHI. The contributions of woodland, wetland and water types are

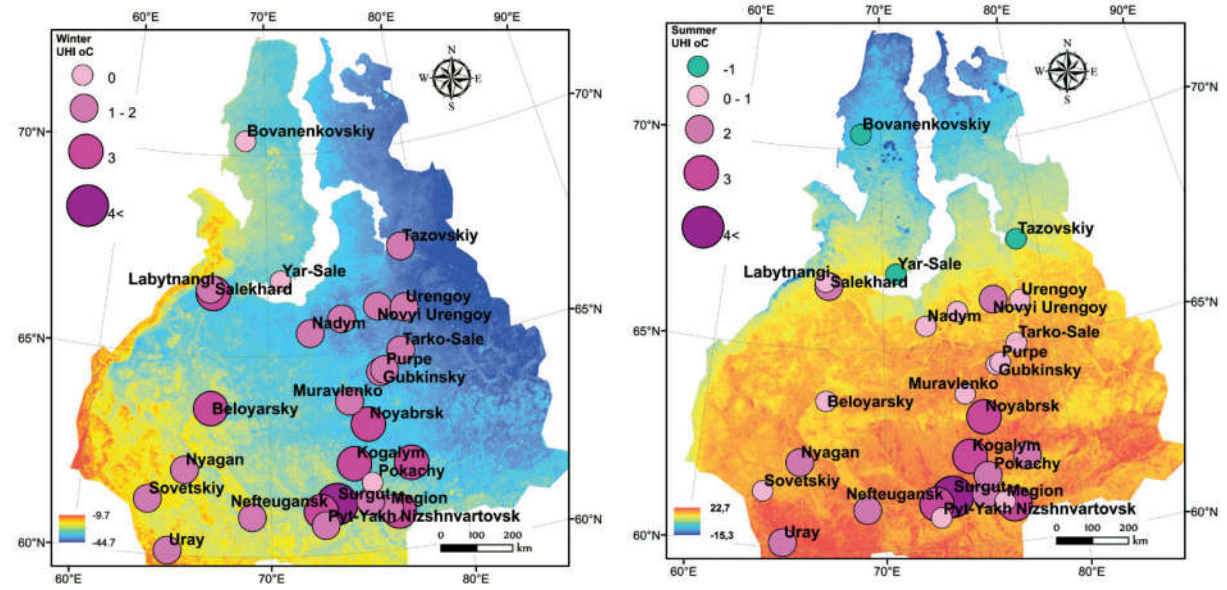

(a) (b)

Fig. 1. Map of the Northern Western Siberia with the SUHI in the 28 cities: (a) the mean winter background LST (colour shading) and SUHI (coloured circles); (b) the mean summer background LST and SUHI. The summer season includes June, July and August, whereas the winter season includes December, January and February

Table 2. Studied cities in the northern West Siberia region and their relevant characteristics

City name	Pop. (x10^3)	Area (km^2)	Long. (deg.)	Lat. (deg.)	SUHI JJA (K)	SUHI DJF (K)	LST JJA (°C)	LST DJF (°C)
Beloyarsky	49	33	66,68	63,71	1,45	2,59	15,63	-25,68
Bovanenkovskiy	4	0,5	68,54	70,36	0,00	0,00	7,84	-26,17
Gubkinsky	26	18	76,46	64,44	0,80	1,66	15,22	-28,06
Khanty-Mansyisk	93	22	69,02	61,01	1,50	2,19	16,72	-22,81
Kogalym	61	79	74,54	62,25	2,89	3,33	16,07	-26,54
Labytnangi	26	12	66,42	66,66	1,19	1,89	13,40	-26,68
Langepas	43	19	75,18	61,26	1,92	1,83	16,40	-26,00
Megion	49	6	76,11	61,04	1,33	1,59	17,14	-24,16
Muravlenko	33	14	74,53	63,79	1,21	1,64	16,01	-27,18
Nadym	46	10	72,53	65,54	1,32	1,78	14,65	-27,13
Nefteugansk	126	30	72,60	61,09	2,62	2,79	17,19	-24,76
Nizshnevartovsk	266	76	76,55	60,94	3,30	3,94	17,21	-25,26
Novyi Urengoy	116	64	76,83	66,04	1,56	2,02	15,16	-28,74
Noyabrsk	107	69	75,45	63,19	3,20	2,69	15,26	-26,75
Nyagan	56	22	65,40	62,14	2,41	2,19	16,13	-23,49
Pangody	11	8	74,52	65,87	1,14	1,55	14,09	-28,82
Pokachy	17	10	75,60	61,74	1,93	0,43	17,22	-26,07
Purpe	10	9	76,70	64,49	0,67	1,06	15,59	-27,87

Pyt-Yakh	41	23	72,82	60,74	1,17	1,72	16,52	-24,60
Raduzhnyi	43	123	77,47	62,11	2,37	3,03	15,91	-27,26
Salekhard	48	17	66,60	66,53	2,28	3,29	12,86	-26,27
Sovetskiy	28	14	63,57	61,37	1,38	1,16	16,60	-22,46
Surgut	332	54	73,41	61,25	3,64	5,97	17,69	-22,97
Tarko-Sale	21	7	77,79	64,92	0,93	0,93	14,82	-29,23
Tazovskiy	7	6	78,71	67,48	0,28	0,79	12,19	-29,16
Uray	40	31	64,77	60,12	1,54	1,30	17,08	-21,56
Urengoy	11	8	78,36	65,97	1,02	0,73	13,49	-29,55
Yar-Sale	7	1	70,83	66,87	0,00	0,00	11,38	-27,60

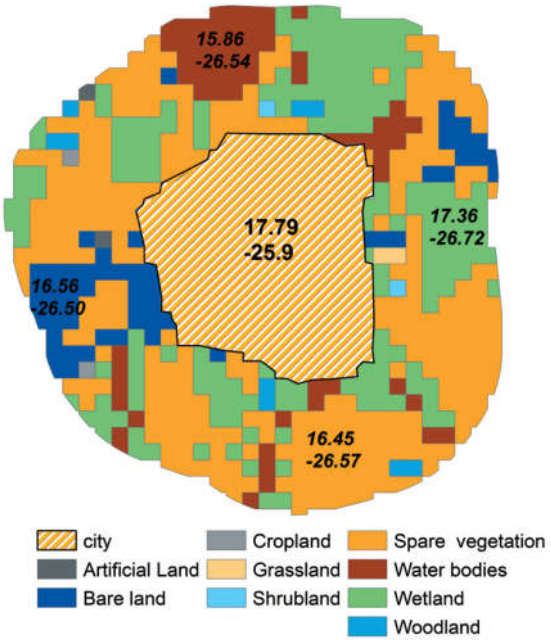

Fig. 2. Land cover (LC) types mapped for the small city of Pokachy. The colour coding shows the different aggregated LC types. The numbers indicate the summer (positive) and the winter (negative) mean LST for the given LC type in the buffer. Details could be found in the text

much smaller (or even negative) than would be expected from their land fraction cover. To further look at these relationships, we studied the SUHI intensity dependence on each LC type. Fig. 5 reveals that there is no clear dependence for each given LC type. At the same time, both the averaged SUHI and the scatter of ΔT_i strongly vary with the LC type. The non-vegetated LC types support the largest SUHI scatter, whereas grassland and cropland support the smallest scatter.

Discussion on the local climates of the LC types

The local climates are shaped by the thermal and aerodynamical features of the surface, by soil moisture and evapotranspiration from the vegetation canopy. Low surface albedo of boreal forest and shrubland, particularly in winter, creates sharp LST contrasts with other LC types. The differences of upper soil moisture shift the balance between latent and sensible heat fluxes sharing a limited amount of incoming heat. Boreal woodland and shrubland, particularly the dark coniferous forest, absorb a larger share of incoming solar radiation than the lighter urban surfaces and other natural LC types (Bonan et al. 1992; Bonan 2008). The surface albedo (from MODIS) of snow covered grassland is 0.7 in the region, whereas it is only 0.5 in the forest area and less than 0.4 without the

snow cover (Atlaskina et al. 2015). Lee et al. (2011) and Li et al. (2015) demonstrated that the boreal forest is generally warmer than other surface types. Thus, the boreal forest reduces the apparent SUHI if the urban area itself does not includes significant forest patches. Spatial heterogeneity of vegetation trends in the region was studied in Miles and Esau (2016). The role of warmer water surface and wetlands becomes important in the northernmost settlements where it reduces the apparent SUHI intensities in Bovanenkovskiy, Yar-Sale and Tazovskiy in summertime, and in Megion and Novyi Urengoy in wintertime.

The winter SUHI is less sensitive to the LC types in the urban buffer. The direct anthropogenic heating in the cold climate cities may reach 50 W m^{-2} and even more locally in severe climate conditions of more densely populated cities (Flanner 2009). This anthropogenic flux exceeds the natural urban heat forcing and supports the winter SUHI in the NWS cities despite less contrasting snow-covered surface.

Discussion on the LST – SAT differences

Recent comprehensive assessments of the LST – SAT differences by Yang et al. (2017) and Nielsen-Englyst et al. (2018) help to understand the physical factors and seasonality of the LST deviations. As Zilitinkevich and Esau (2005) have shown, these differences remain small in convective and near-neutral atmosphere, which can be associated with the positive surface heat balance. The differences rapidly increase in stably-stratified atmosphere, which can be associated with the negative surface heat balance (Esau et al. 2012; Davy and Esau 2014). Thus, increasing atmospheric stability leads to progressively larger cold bias in the LST with respect to the SAT. The periods of diurnal and seasonal cycle, which

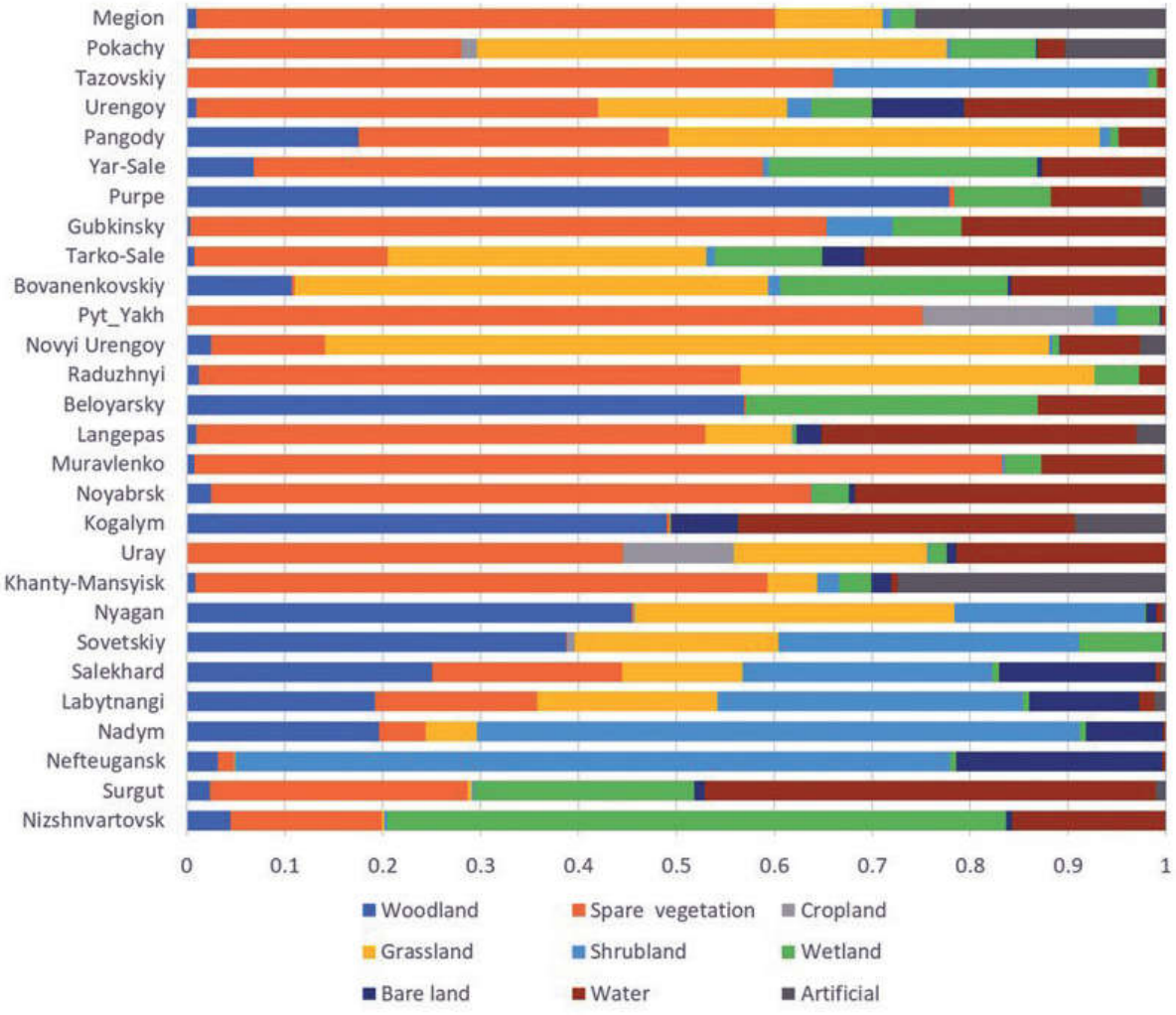

Fig. 3. Composition of the aggregated CCI LC types in the 2 km buffers around the 28 cities in the NWS

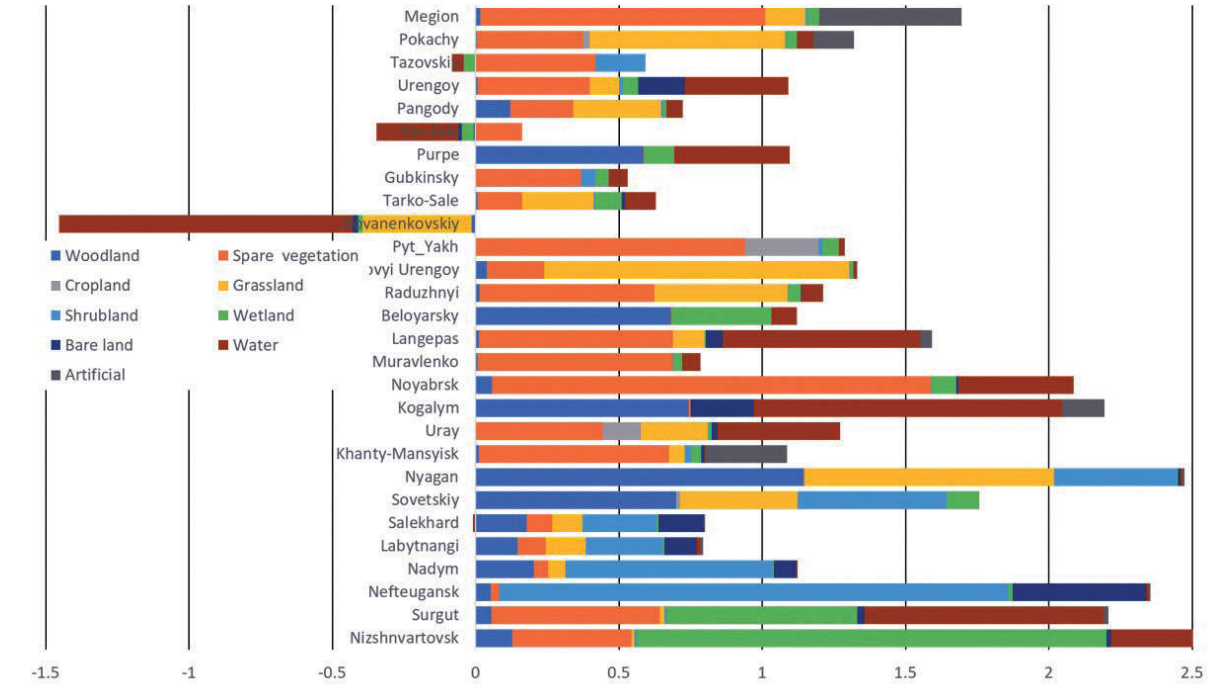

(a) Summer SUHI

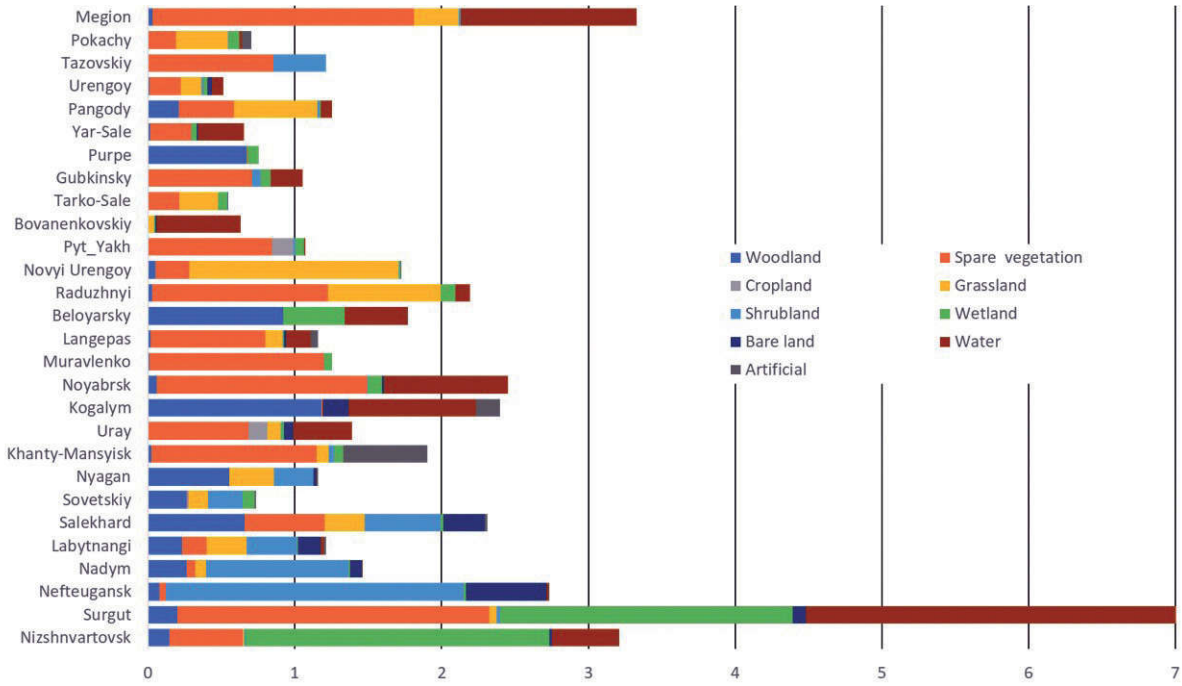

(b) Winter SUHI

Fig. 4. Partial contributions, $f_i\Delta T_i$, of the aggregated LC types into the total SUHI intensity, ΔT for the 28 cities in the NWS region. The contribution is given in Kelvins. The negative values indicate that the specific LC types are locally warmer than the urban area

are dominated by the stable stratification, will show the negative LST bias.

We compared the MODIS LST of the urban pixel and the nearly collocated SAT observations at the WMO station 23848 (Nefteyugansk airport) over the period 2006-2014. The analysis revealed that the summertime LST was 0.0 K (2007) to 2.5 K (2012) higher than the SAT. The average LST – SAT difference was +1.2 K. The wintertime LST of the urban pixel was 1.0 K (2010) to 7.5 K (2012) lower than the SAT. The average difference was -2.9 K. The urban LST is higher than that of the natural background in both seasons (see ME17 and Table 2). Therefore, the SAT comparison with the natural pixels would constitute the smaller LST – SAT

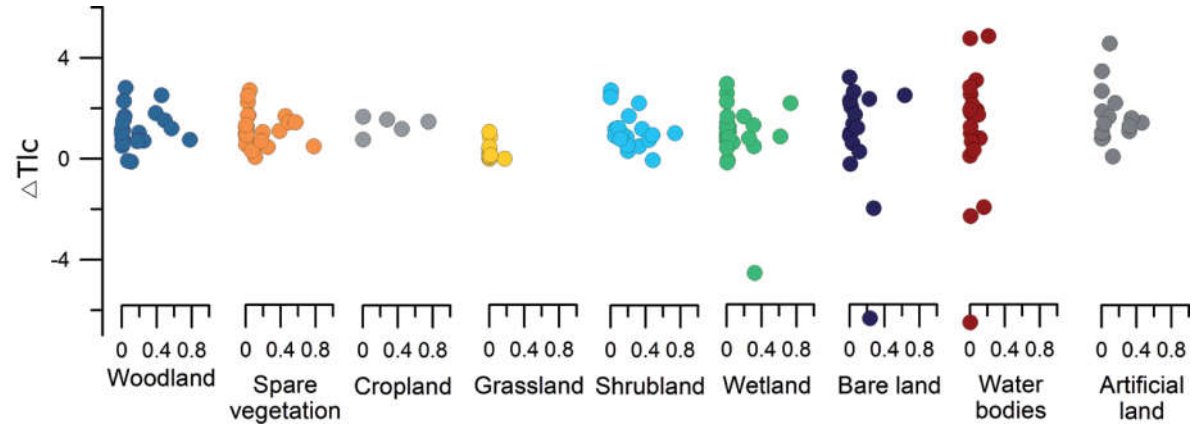

(a) Summer

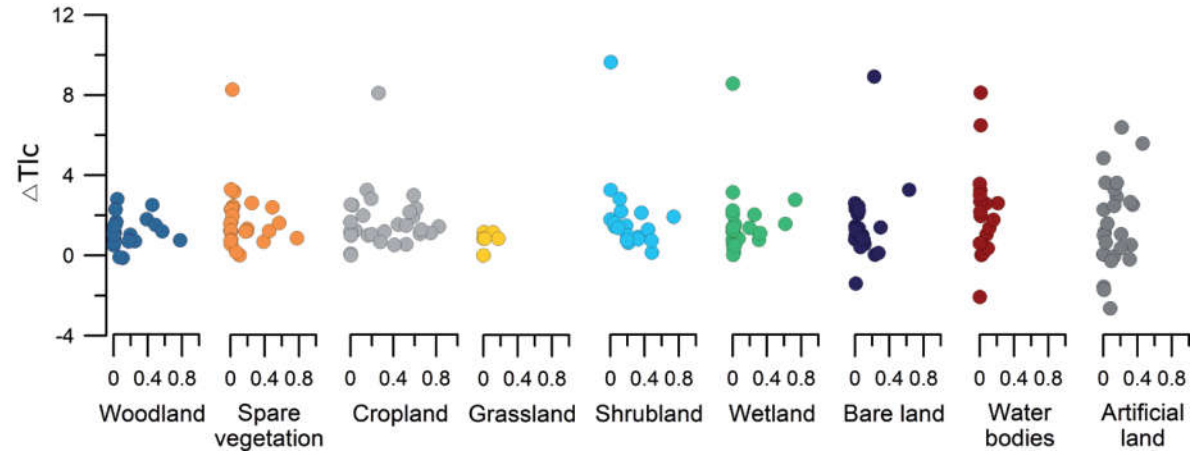

(b) Winter

Fig. 5. Dependence of the partial SUHI intensity, ΔTι [K], on the buffer fraction covered with the given LC type for the 28 cities in the NWS

differences in the summertime and even larger difference in the wintertime.

There are no pairs of close urban-rural SAT observations in the region. Therefore, we can only speculatively extrapolate our understanding to the SUHI – UHI relationships. The SUHI in this study is unlikely to be significantly different from the more traditional urban canopy UHI in summertime. Moreover, the summertime SUHI should not exhibit significant sensitivity to the stratification over the different land use – land cover types. On the contrary, the wintertime SUHI is expected to be much colder than the corresponding UHI. The region of this study is known for its persistent negative surface heat balance and frequent clear-sky anti-cyclonic weather (e.g. Konstantinov et al. 2018). Considering sites with similar winter conditions from the Nielsen-Englyst et al. (2018) study, we expect the wintertime LST over open natural landscapes to be 2-3 K lower than the LST in the urban area. This question needs further investigation.

CONCLUSIONS

This study presents the analysis of the exogenous factors responsible for the apparent SUHI in the 28 cities in Northern West Siberia. It considered the quantitative contribution of local climates, specific for the aggregated LC types in the 2 km buffer of the urban administrative area. The study utilized the MODIS LST data product for the period of 2001-2015. The CCI LC types were aggregated in 9 coarser LC types in this study.

The MODIS LST analysis in ME17 revealed significant and persistent warm LST anomalies in the cities. ME17 found a strong statistical dependence (R^2 = 0.73) on the single endogenies factor, namely, the size of city population. It was suggested that the background LC types, such as boreal forest,

could play a significant role in scaling of the SUHI. Here, we studied and quantified that suggestion. No clear dependence between the partial SUHI intensity and the area fraction occupied by the given LC type was found. Nevertheless, the major contribution to the apparent SUHI was revealed for water, spare vegetation, grassland and shrubland.

Different partial SUHI intensity can explain relatively small summer LST anomalies in the high latitude cities as compared to their counterparts in lower latitudes. Indeed, the NWS cities are surrounded by dark natural vegetation (forest and shrub), as cropland is practically not present. The higher urban albedo counteracts warming, making the LST differences less significant. The mechanisms and pathways of the SUHI maintenance cannot be solely inferred from the remote sensing data. Their further understanding requires numerical experiments with turbulence-resolving models.

The large and persistent SUHI in the NWS cities may have significant ecosystem as well as socio-economic impacts. Esau et al. (2016) showed that the vegetation productivity generally increasing in and around those 28 cities. Following analysis of the NWS climate change, it is reasonably to expect that the SUHI will further reduce the bearing capacity of frozen soils. The work of Zhou et al. (2004) suggests that shifts in the vegetation phenological cycle should be also observed. Such an expected impact calls for concrete in depth investigations of the SUHI effects in each city as well as for urban planning and policy measures to minimize those effects.

ACKNOWLEDGEMENTS

This work was supported by the Belmont Forum and Norwegian Research Council project HIARC: *Anthropogenic Heat Islands in the Arctic: Windows to the Future of the Regional Climates, Ecosystems, and Societies (no. 247468).*

REFERENCES

Atlaskina K., Berninger F., de Leeuw G. (2015). Satellite observations of changes in snow-covered land surface albedo during spring in the Northern Hemisphere. The Cryosphere. Vol. 9. P. 1879-1893.

Barichivich J., Briffa K.R., Myneni R., van der Schrier G., Dorigo W., Tucker C.J., Osborn T.J., Melvin T.M. (2014). Temperature and snow-mediated moisture controls of summer photosynthetic activity in northern terrestrial ecosystems between 1982 and 2011. Remote Sens. Vol. 6. P. 1390-1431.

Bonan G.B., Pollard D., Thompson S.L. (1992). Effects of boreal forest vegetation on global climate. Nature. Vol. 359. P. 716-718.

Bonan G.B. (2008). Forests and Climate Change: Forcings, Feedbacks, and the Climate Benefits of Forests. Science. Vol. 320. P. 1444-1449.

Brunsell N.A., Mechem D.B., Anderson M.C. (2011). Surface heterogeneity impacts on boundary layer dynamics via energy balance partitioning. Atmos. Chem. Phys. Vol. 11. P. 3403-3416.

Chen X., Su Z., Ma Y., Cleverly J., Liddell M. (2017). An Accurate Estimate of Monthly Mean Land Surface Temperatures from MODIS Clear-Sky Retrievals. J. Hydrometeorol. Vol. 18. P. 2827-2847.

Comiso J. C. (2003). Warming Trends in the Arctic from Clear Sky Satellite Observations. J. Climate. Vol. 16. P. 3498-3510.

Clinton N., Gong P. (2013). MODIS detected surface urban heat islands and sinks: Global locations and controls. Remote Sens. Env. Vol. 134. P. 294-304.

Davy R., Esau I., Chernokulsky A., Outten S., Zilitinkevich S. (2017). Diurnal asymmetry to the observed global warming. Int. J. Climatol. Vol. 37. P. 79-93.

Davy R., Esau I. (2014). Surface air temperature variability in global climate models. Atmos. Sci. Letters. Vol. 15. P. 13-20.

Davy R., Esau I. (2016). Differences in the efficacy of climate forcings explained by variations in atmospheric boundary layer depth. Nature Comm. Vol. 7. Art. ID. 11690.

Davy R., Esau I., Chernokulsky A., Outten S., Zilitinkevich S. (2017). Diurnal asymmetry to the observed global warming. Int. J. Climatol. Vol. 37. P. 79-93.

Dudorova N., Belan B. (2015). Thermal balance of the underlying surface in Tomsk during 2004–2005. Atmos. Ocean Optics. Vol. 28. No. 4. P. 318-327.

Esau I., Davy R., Outten S. (2012). Complementary explanation of temperature response in the lower atmosphere. Env. Res. Letters. Vol. 7. Art. ID. 044026.

Esau I., Miles V. (2016). Warmer urban climates for development of green spaces in northern Siberian cities. Geogr. Env. Sustain. Vol. 9. P. 48-62.

Esau I., Miles V.V., Davy R., Miles M.W., Kurchatova A. (2016). Trends in normalized difference vegetation index (NDVI) associated with urban development in northern West Siberia. Atmos. Chem. Phys. Vol. 16. P. 9563–9577.

Flanner M.G. (2009). Integrating Anthropogenic Heat Flux with Global Climate Models. Geophys. Res. Lett. Vol. 36. No. 2. Art. ID. L02801.

He J. F., Liu J. Y., Zhuang D. F., Zhang W., Liu M. L. (2007). Assessing the effect of land use/land cover change on the change of urban heat island intensity. Theor. Appl. Climatol. // Vol. 90. P. 217-226.

Hachem S., Duguay C. R., Allard M. (2012). Comparison of MODIS-derived land surface temperatures with ground surface and air temperature measurements in continuous permafrost terrain. The Cryosphere. Vol. 6. P. 51-69.

Heleniak T.E. (2009). The role of attachment to place in migration decisions of the population of the Russian North. Polar Geography. Vol. 32. P. 31-60.

Hinkel K.M., Nelson F.E. (2007). Anthropogenic heat island at Barrow, Alaska, during winter: 2001–2005. J. Geophys. Res. Vol. 112. Art. ID. D06118

Hu Y., Jia G. (2010). Influence of land use change on urban heat island derived from multi-sensor data. Int. J. Climatol. Vol. 30. P. 1382-1395.

Grebenets V.I., Streletskiy D., Shiklomanov N. (2012). Geotechnical safety issues in the cities of polar regions. Geography Env. Sustainability. Vol. 5. P. 104-119.

Imhoff M.L., Zhang P., Wolfe R.E., Bounoua L. (2010). Remote sensing of the urban heat island effect across biomes in the continental USA. Remote Sensing Env. Vol. 114. P. 504–513.

Jin M., Dickinson R. E. (2010). Land surface skin temperature climatology: benefitting from the strengths of satellite observations. Enviromen. Res. Lett. Vol. 5. ID. 044004

Khrustalyov L., Davidova I. (2007). Forecast of climate warming and account of it at estimation of foundation reliability for buildings in permafrost zone. Earth Cryosphere. Vol. 11. P. 68-75. (in Russian)

Konstantinov P.I., Grishchenko M.Y., Varentsov M.I. (2015). Mapping Urban Heat Islands of Arctic Cities Using Combined Data on Field Measurements and Satellite Images Based on the Example of the City of Apatity (Murmansk Oblast). Izvestiya, Atmos. Ocean. Phys. Vol. 51. P. 992–998.

Konstantinov P., Varentsov M., Esau I. (2018). A high density urban temperature network deployed in several cities of Eurasian Arctic. Environ. Res. Lett. Vol. 13. ID. 075007.

Kottek M., Grieser J., Beck C., Rudolf B., Rubel F. (2006). World Map of the Köppen-Geiger climate classification updated. Meteorol. Zeitschrift. Vol. 15. P. 259–263.

Lapenis A., Shvidenko A., Shepaschenko D., Nilsson S., Aiyyer A. (2005). Acclimation of Russian forests to recent changes in climate. Global Change Biology. Vol. 11. P. 2090-2102.

Lee X., Goulden M.L., Hollinger D.Y. et al. (2011). Observed increase in local cooling effect of deforestation at higher latitudes. Nature. Vol. 479. P. 384-387.

Lemonsu A., Bélair S., Mailhot J., Benjamin M., Morneau G., Harvey B., Chagnon F., Jean M., Voogt J. (2008). Overview and First Results of the Montreal Urban Snow Experiment 2005. J. Appl. Meteorol. Climatol. Vol. 47. P. 59-75.

Li Z.-L., Tang B.-H., Wu H., Ren H., Yan G., Wan Z., Trigo I.F., Sobrino J.A. (2013). Satellite-derived land surface temperature: Current status and perspectives. Remote Sensing Env. Vol. 131. P. 14–37.

Li Y., Zhao M., Motesharrei S., Mu Q., Kalnay E., Li S. (2015). Local cooling and warming effects of forests based on satellite observations. Nature Comm. Vol. 6. Art. ID. 6603.

Li B., Liu Z., Nan Y., Li S., Yang Y. (2018). Comparative Analysis of Urban Heat Island Intensities in Chinese, Russian, and DPRK Regions across the Transnational Urban Agglomeration of the Tumen River in Northeast Asia. Sustainability. Vol. 10. ID. 2637

Lowry W. P. (1977). Empirical Estimation of Urban Effects on Climate: A Problem Analysis. J. Appl. Meteorol. Vol. 16. P. 129-135.

Magee N., Curtis J., Wendler G. (1999). The Urban Heat Island Effect at Fairbanks, Alaska. Theor. Appl. Climatol. Vol. 64. P. 39-47.

Makhrovskaya A.V., Vaytens M.Y., Panov L.K., Belinskiy A.Y. (1977). Urban planning and construction in the kola north (Part I). Polar Geography. Vol. 1. P. 205-216.

Metz M., Andreo V., Neteler M. (2017). A New Fully Gap-Free Time Series of Land Surface Temperature from MODIS LST Data. Remote Sens. Vol. 9. P. 1333

Miles V.V., Esau I. (2016). Spatial heterogeneity of greening and browning between and within bioclimatic zones in northern West Siberia. Environ. Res. Lett. doi:10.1088/17489326/11/11/115002

Miles V., Esau I. (2017). Seasonal and Spatial Characteristics of Urban Heat Islands (UHIs) in Northern West Siberian Cities. Remote Sensing. Vol. 9. Art. ID. 989

Mokhov I.I. (2009). Links between urban heat island intensity and its size and urban population. Doklady RAS. Vol. 427. P. 530-533.

Mori K., Sato T. (2015). Evaluating the Role of Snow Cover in Urban Canopy Layer on the Urban Heat Island in Sapporo, Japan with a Regional Climate Model. J. Meteorol. Soc. Japan. Vol. 93. P. 581-592.

Muster S., Langer M., Abnizova A., Young K., Boike J. (2015). Spatio-temporal sensitivity of MODIS land surface temperature anomalies indicates high potential for large-scale land cover change detection in Arctic permafrost landscapes. Remote Sens. Environ. V. 168. P. 1-12.

Nielsen-Englyst P., Høyer J.L., Madsen K.S., Dybkjær G., Tonboe R., Alerskans E. (2018). In situ observed relationships between skin temperatures and 2m air temperatures in the Arctic. The Cryosphere Discussions. doi: 10.5194/tc-2018-150

Oke T.R. (1973). City size and the urban heat island. Atmos. Env. Vol. 7. P. 769-779.

Peng S., Piao S., Ciais P., Friedlingstein P., Ottle C., Bréon F.-M., Nan H., Zhou L., Myneni R.B. (2012). Surface Urban Heat Island Across 419 Global Big Cities. Env. Sci. Technol. Vol. 46. P. 796-703.

Schwarz N., Lautenbach S., Seppelt R. (2011). Exploring indicators for quantifying surface urban heat islands of European cities with MODIS land surface temperatures. Remote Sensing of Env. Vol. 115. P. 3175-3186.

Shastri H., Barik B., Ghosh S., Venkataraman C., Sadavarte P. (2017). Flip flop of day-night and summer-winter surface urban heat island intensity in India. Scientific Reports. Vol. 7. ID. 40178

Shiklomanov N.I., Streletskiy D.A., Swales T.W., Kokorev V.A. (2016). Climate change and stability of urban infrastructure in Russian permafrost regions: prognostic assessment based on GCM climate projections. Geograph. Rev. P. 1-18.

Smoliak B.V., Snyder P.K., Twine T.E., Mykleby P.M., Hertel W.F. (2015). Dense Network Observations of the Twin Cities Canopy-Layer Urban Heat Island. J. Appl. Meteorol. Climatol. Vol. 54. P. 1899-1917.

Stewart I.D. (2011). A systematic review and scientific critique of methodology in modern urban heat island literature. Int. J. Climatol. Vol. 31. P. 200-217.

Streletskiy D.A., Shiklomanov N., Grebenets V. (2012). Changes of foundation bearing capacity due to climate warming in northwest Siberia. Earth Cryosphere. Vol. 16. P. 22-32. (in Russian)

Sun C.-Y., Lin H.-T. (2005). Urban heat island intensity in subtropical Taiwan. Proc. World Sustainable Building Conf. Tokyo. 27-29 Sep. P. 2296-2301.

Tan M., Li X. (2015). The effects of settlement size on urban heat islands in fairly uniform geographic areas. Habitat Int. Vol. 49. P. 100-106.

Tomlinson C. J., Chapman L., Thornes J. E., Baker C. J. (2012). Derivation of Birmingham's summer surface urban heat island from MODIS satellite images. Int. J. Climatol. Vol. 32. P. 214-224.

Varentsov M.I., Konstantinov P.I., Samsonov T.E., Repina I.A. (2014). Investigation of the urban heat island phenomenon during polar night based on experimental measurements and remote sensing of Norilsk city. Sovremennye Problemy Distantsionnogo Zondirovaniya Zemli iz Kosmosa. Vol. 11. P. 329–337 (in Russian).

Voogt J., Oke T. (2003). Thermal remote sensing of urban climates. Remote Sens. Environ. Vol. 86. P. 370-384.

Wang W., Liang S., Meyers T. (2008). Validating MODIS land surface temperature products using long-term nighttime ground measurements. Remote Sensing Env. Vol. 112. P. 623–635.

Yang Y., Cai W., Yang J. (2017). Evaluation of MODIS Land Surface Temperature Data to Estimate Near-Surface Air Temperature in Northeast China. Remote Sens. Vol. 9. P. 410.

Yuan F., Marvin E. B. (2007). Comparison of impervious surface area and normalized difference vegetation index as indicators of surface urban heat island effects in Landsat imagery. Remote Sens. Environ. Vol. 106. No. 3. P. 375–386.

Zilitinkevich S., Esau I. (2005). Resistance and Heat Transfer Laws for Stable and Neutral Planetary Boundary Layers: Old Theory, Advanced and Re-evaluated. Q. J. R. Meteorol. Soc. Vol. 131. P. 1863-1892.

Zhang H., Zhang F., Zhang G., He X., Tian L. (2016). Evaluation of cloud effects on air temperature estimation using MODIS LST based on ground measurements over the Tibetan Plateau. Atmos. Chem. Phys. Vol. 16. P. 13681-13696.

Zhang P., Imhoff M.L., Wolfe R.E., Bounoua L. (2010). Characterizing urban heat islands of global settlements using MODIS and nighttime lights products. Canadian J. Remote Sensing. Vol. 36. No. 3. P. 185-196.

Zhao L., Lee X., Smith R.B., Oleson K. (2014). Strong contributions of local background climate to urban heat islands. Nature, Vol. 511. P. 214-219.

Zhou L., Dickinson R.E., Tian Y., Fang J., Li Q., Kaufmann R.K., Tucker C.J., Myneni R.B. (2004). Evidence for a significant urbanization effect on climate in China. Proc. Nat. Acad. Sci. USA. Vol. 101. 9540–9544.

Zhou B., Rybski D., Kropp J.P. (2013). On the statistics of urban heat island intensity. Geophys. Res. Lett. Vol. 40. 5486–5491.

Zhou D., Zhao S., Zhang L., Sun G., Liu Y. (2015). The footprint of urban heat island effect in China. Sci. Reports. Vol. 5. P. 11160.

Received on October 27th, 2017 Accepted on July 31st, 2018

AUTHORS

Igor Esau graduated in meteorology and climatology in 1992 from the Tomsk State University. He received a Ph.D. in 1996 at the Institute for Numerical Mathematics of the Russian Academy of Science and in 2003 at the Uppsala University in Sweden. Since 2003, he is working at the Nansen Environmental and Remote Sensing Centre in Norway (www.nersc.no) where he presently leads a Climate Processes group. His main fields of interest include: the role of the planetary boundary layer in the earth's climate system; numerical modeling of the atmospheric turbulence; and societal effects of the micro-climate processes. The most significant recent publication: Davy R., Esau I. (2016). Differences in the efficacy of climate forcings explained by variations in atmospheric boundary layer depth, Nature Communications, Vol. 7, 11690, doi:10.1038/ncomms11690

Victoria Miles graduated the St. Petersburg Forestry Academy in 1993. She received a Ph.D. in 1998 at the St. Petersburg State University. Since 2002, she is working at the Nansen Environmental and Remote Sensing Centre in Norway (www.nersc.no) where she studies climate processes with the methods of the satellite remote sensing image analysis and geo-information systems. Her main fields of interest include: forest studies; high-latitude vegetation and land use mapping; glaciological processes. The most significant recent publication: Miles V. and Esau I. (2017) Seasonal and Spatial Characteristics of Urban Heat Islands (UHIs) in NorthernWest Siberian Cities. // Remote Sensing, 9, 989